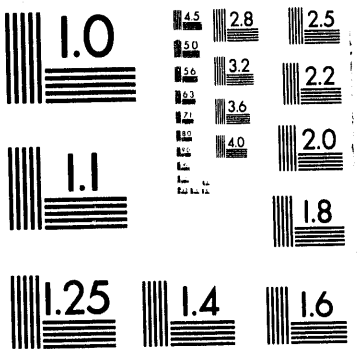
1.0
1.1
1.25
1.4
1.6
1.8
2.0
2.2
2.5
2.8
3.2
3.6
4.0
4.5
5.0
5.6
6.3
7.1
8.0
9.0

1 of 1

71811

ANL/PHY/PP--71811

Chiral symmetry and the threshold $\gamma p \to \pi^0 p$ reaction

T.-S H. Lee

Physics Division, Argonne National Laboratory, Argonne, Il. 60439

B. C. Pearce

TRIUMF, 4004 Wesbrook Mall, Vancouver, British Columbia, Canada V6T 2A3

The threshold $\gamma p \to \pi^0 p$ reaction is investigated by using a chiral invariant πN model in a unitary, gauge invariant, dynamical calculation based on a chiral Lagrangian. It is shown that the chiral invariant πN final state interaction significantly suppresses the E_{0+} amplitude from the value $-2.4 \times 10^{-3} m_\pi^{-1}$ predicted by the low energy theorem to $-0.66 \times 10^{-3} m_\pi^{-1}$. We discuss questions concerning the implications of the present results in interpreting the recent Mainz data[1] and their multipole analysis. The experimental accuracy needed for investigating chiral symmetry breaking is illustrated.

In a recent paper, Beck *et al.* [1] reported a measurement of the photo-production of neutral pions (π^0) on the nucleon near threshold. This experiment, performed at Mainz, was more precise than the previous Saclay experiment[2] in measuring angular distributions. By keeping only the real parts of the s- and p-wave multipoles to fit the cross sections, it was concluded that the E_{0+} amplitude at threshold is significantly suppressed from the value predicted by the well-established low energy theorem. This result has stimulated great interest[3,4,5,6] in investigating the dyn- ical origin of chiral symmetry breaking. In Ref. 6, Sachäfer and Weise have explored its possible connection to some basic parameters of the nucleon.

To draw definite conclusions from these interesting developments, it is important to emphasize that some of the observed deviation from the low energy theorem prediction is due to the πN final state interaction (FSI), as has been studied by several authors.[7,8,9,10] To investigate chiral symmetry breaking, it is essential to calculate properly the chiral invariant part of the FSI. In this paper, we address this issue within the Hamiltonian formulation developed by Nozawa, Blankleider and Lee[11] and, independently, by Yang.[9] In these two models, chiral symmetry is taken into account properly in defining the basic mechanisms of the electromagnetic productions of pions. Specifically, at threshold the current matrix element (in the absence of FSI) is dominated by the pseudo-vector coupling. The main drawback of these two works is that the FSI was calculated using separable πN potentials which are not constrained by chiral symmetry. Their predicted FSI values are at most suggestive in nature, as stressed at the end of Ref. 8.

Perhaps the most tractable approach to implement chiral symmetry in evaluating πN rescattering is to start with an effective chiral invariant Lagrangian. The attempts made in the 1970's, for example by Gervais and Lee[12] and Lin and Wiley,[13] were to calculate the one-loop corrections and use suitable Pade approximations to generate higher order effects and unitarize the resulting amplitude. These earlier works qualitatively reproduce the πN phase shifts. But it appears to be very difficult to go beyond the one-loop level and achieve an accurate description of the πN data. In this work, we take an alternative to these earlier

approaches and calculate the πN rescattering by using a chiral invariant meson-exchange πN model developed by Pearce and Jennings.[14]

The essence of the πN model of Ref. 14 is to employ a three-dimensional reduction of Bethe-Salpeter equation to deduce a πN potential starting with an effective chiral invariant Lagrangian. The potential is calculated from the Feynman amplitudes of the nucleon-pole, crossed nucleon, Δ-pole, crossed Δ and ρ and σ exchange terms. Appropriate form factors are introduced to regularize matrix elements of the πN potential at high momenta. The resulting range of the crucial πNN form factor is similar to that of the cloudy bag model.[15] In addition to giving an excellent description of all s- and p-wave πN phase shifts up to about 400 MeV pion laboratory energy, the model correctly reproduces the soft pion relation between the s-wave scattering lengths. The s-wave phase shifts of this model are illustrated in the upper part of Fig. 1. In the lower part of Fig. 1, we show that, in the limit $m_\pi \to 0$, the calculated isospin-odd πN scattering length vanishes linearly while the isospin-even scattering length vanishes quadratically, as required by chiral symmetry. This is an important ingredient for the present study. All calculations based on purely phenomenological πN potentials do not account for chiral symmetry.

To proceed, we recall the Hamiltonian formulation developed in Ref. 11 to write the considered π^0 photo-production amplitude in the following form

$$M_{\pi^0 p \leftarrow \gamma p}(\vec{k_0}, \vec{q}) = B_{\pi^0 p \leftarrow \gamma p}(\vec{k_0}, \vec{q}) + (FSI)_{\pi^0 p} + (FSI)_{\pi^+ n}, \tag{1}$$

where $\vec{q}$ and $\vec{k_0}$ are respectively the initial photon and final pion momenta. The Born term, B, is calculated from the lowest order Feynman amplitudes of an effective Lagrangian describing interactions among $\pi, N, \Delta, \rho, \omega$ and γ. They are given explicitly in Ref. 11. The final state interaction terms (FSI) of Eq. (1) are calculated from

$$(FSI)_{\pi N} = \int d\vec{k} \frac{T_{\pi_0 p \leftarrow \pi N}(\vec{k_0}, \vec{k}, E) B_{\pi N \leftarrow \gamma p}(\vec{k}, \vec{q})}{E - E_N(k) - E_\pi(k) + i\epsilon}, \tag{2}$$

where the πN half-off-shell t-matrix is generated from the following Lippmann-Schwinger

equation

$$T_{\pi N,\pi N}(\vec{k}',\vec{k},E) = v_{\pi N,\pi N}(\vec{k}',\vec{k},E) + \int d\vec{k}\frac{v_{\pi N,\pi N}(\vec{k}',\vec{k}'',E)T_{\pi N,\pi N}(\vec{k}'',\vec{k},E)}{E - E_N(k'') - E_\pi(k'') + i\epsilon}. \tag{3}$$

Here $v_{\pi N,\pi N}$ is a πN potential. It is determined by vertices $\pi N \leftrightarrow N, \Delta$ and a background πN potential. More detailed formulations can be found in Ref. 11. The gauge invariance and unitarity of the photo-production amplitude Eq. (1) are also discussed in detail there. For the present purposes, Eqs. (1)–(3) are sufficient.

The Born amplitude B of Eq. (1) contains the standard pseudo-vector pion coupling terms and hence, in the absence of FSI, the calculations at threshold are in excellent agreement with the low energy theorem predictions (the effect due to vector mesons and Δ are very small at threshold, as explicitly shown in Tables II and III of Ref. 8). To fully account for the dynamical consequences of chiral symmetry, we need to generate the off-shell πN t-matrix from a chiral invariant πN potential in a way that preserves chiral symmetry. This is achieved by casting the πN scattering equation of Ref. 14 into the form of Eq. (3). In doing this, the main step is to approximate the lower-lower component of the "smooth" πN propagator of Ref.14. This approximation is exact at the pole in the propagator and does not alter the results of Ref. 14 in any significant way. With some straightforward derivations,[16] Eq. (3) can then be derived from the formulation of Ref. 14. The resulting πN potential can be written as

$$v_{\pi N,\pi N}(\vec{k}',\vec{k},E) = \Gamma^{1/2}(k',E)\bar{u}(\vec{k}',E,s')\mathcal{V}(\vec{k}',\vec{k},E)u(\vec{k},E,s)\Gamma^{1/2}(k,E). \tag{4}$$

where $\mathcal{V}$ is the πN potential used in Ref. 14. Here we have introduced

$$\Gamma(k,E) = \frac{4m_N E^2[E_N(k)+E_\pi(k)]^2}{(2\pi)^3 E[E+E_N(k)+E_\pi(k)][E^2(E_N(k)+E_\pi(k))^2-(m_N^2-m_\pi^2)^2]}, \tag{5}$$

and $u(\vec{k},E,s)$ is an "off-shell spinor" defined by

$$u(\vec{k},E,s) = \sqrt{\frac{E_N(k_0)+m_N}{2m_N}}\begin{pmatrix} \chi_s \\ \dfrac{\sigma\cdot\vec{k}\chi_s}{E_N(k_0)+m_N} \end{pmatrix}, \tag{6}$$

where k_0 is the on-shell momentum corresponding to energy E and χ_s is the two-component spinor corresponding to spin projection s. Numerically, the t-matrix obtained by solving Eq. (3) with the potential given by Eq. (4) reproduce within 2% the results of Ref. 14. Thus we have transformed the off-shell scattering amplitude constructed in Ref. 14 into a form suitable for the calculations based on Eqs. (1)–(3).

With the πN off-shell t-matrix specified above, the model has three free parameters: G_M and G_E of the magnetic $M1$ and electric $E2$ transitions of the $\gamma N \leftrightarrow \Delta$ vertex, and a cutoff parameter Λ of a monopole form factor $F_{cut}(k) = \Lambda^2/(\Lambda^2 + k^2)$ applied to the non-Δ part of the Born term. Note that the cut-off factor $F_{cut}(k)$ is introduced to assure that the current matrix elements are square-integrable and hence the integration in the FSI terms of Eq. (2) is finite. Following Ref. 11, we adjust these three parameters to get the best description of *all* $\gamma N \rightarrow \pi N$ data (including the charged pion data) up to about 400 MeV incident photon energy. The strengths G_M and G_E are strongly constrained by the fits to the data in the Δ region. The over-all energy dependence of the cross sections from the threshold to the Δ region is sensitive to the value of Λ. Therefore, only in a small region of the parameter-space of G_M, G_E and Λ are the fits acceptable. Our fits to the data up to 400 MeV are as good as that of Ref. 8. The resulting parameters are $G_M = 3.065$, $G_E = 0.07$ and $\Lambda = 550$ MeV/c. Note that these parameters are significantly different from that of Ref. 8. It reflects the importance of using a theoretically well-constrained πN off-shell t-matrix in FSI calculation. We will discuss this in detail in a longer paper[16] to follow, along with our extensive results. For the present discussion, we show in Fig. 2 our results (solid curves) for the considered $\gamma p \rightarrow \pi^0 p$ reaction.

The results displayed in Fig. 2 show that the model can describe very well the differential cross section data at all energies above 159 MeV. At lower energies, the predicted cross sections (solid curves in the right hand side of Fig. 2) overestimate the data of Beck *et al.* ,[1] except perhaps in the region of large scattering angle and at the lowest considered energy (146.8 MeV). In Table 1 we list the calculated multipole amplitudes for $l \leq 2$. It is seen

that the M_{1+} amplitude is the largest one at all considered energies. The contribution from this amplitude alone will yield a symmetric bell-shape angular distribution peaked at $\theta = 90°$. The other multipoles are much weaker but they can strongly influence the angular distribution through the interference with the M_{1+} amplitude. In particular, the rising shapes of the calculated angular distributions at 146.8 and 149.1 MeV are mainly due to the interference with the E_{0+} amplitude. This interference effect is much less at higher energies and hence the calculated angular distributions have the shapes predominantly determined by the p-waves. The higher multipole amplitudes listed in Table 1 also play non-negligible roles in determining the cross sections.

It is interesting to explore in which way the discrepancies seen in Fig. 2 (solid curves) can be removed by modifying the calculated multipole amplitudes. We have found that this can *not* be achieved by only modifying the E_{0+} amplitude which is the focus of the studies[3,4,5,6] of chiral symmetry breaking. To bring the calculated magnitudes close to the experimental values at the peaks $\theta \simeq 90°$, it is necessary to weaken the p-wave multipoles by about 20%. The resulting differential cross sections are the dashed curves shown in Fig. 2. More detailed analysis of this p-wave suppression at low energies is clearly needed and will be presented in our future publication.[16]

The predicted E_{0+} amplitude is compared with the low energy theorem prediction in Fig. 3. Its main feature is the cusp structure in the region near 151 MeV. This is due to the opening of the $\pi^+ n$ channel, as discussed in detail in Ref. 8. It is important to emphasize that the FSI suppression of the real part of the E_{0+} amplitude from the low energy theorem prediction shown in Fig. 3 is calculated within the constraints of chiral symmetry. Hence, by comparing the solid curve with that from a multipole analysis of the data, we can determine the chiral symmetry breaking. However, it is inappropriate to use the E_{0+} extracted in Ref. 1 to make such a comparison and draw any conclusion about this important issue. The main uncertainty is because the fit to the data is sensitive to the interference between the E_{0+} and the other multipoles. The theoretical interpretation of their E_{0+} values is therefore closely

related to their extracted p-wave multipoles and the assumptions they made. By using Table 1, we find that the values of $M_1 \equiv 3 \times E_{1+} + M_{1+} - M_{1-} = 2.021$, 2.963, 3.583, 4.175 and 4.730 $\times 10^{-3} m_\pi^{-1}$ for $E_\gamma = 146.8$, 149.1, 151.4, 153.7 and 156.1 MeV respectively. These values are significantly different from those extracted from the analysis of Beck *et al.* (see Fig. 3 of Ref. 1). In addition, the imaginary part of E_{0+} as well as the higher multipoles ($M_{l\pm}$ and $E_{l\pm}$ with $l \geq 2$) are neglected in their analysis. It would be interesting to perform a multipole analysis constrained by the $\iota = 2$ multipoles listed in Table 1($l \geq 3$ multiploes are found to be of much less significant in our calculation). The difference between the resulting E_{0+} and the present chiral invariant calculation results (shown in Fig. 3 and Table 1) would then be the effect due to chiral symmetry breaking. This, however, can not be done reliably unless the quality of data is improved and some polarization measurements are performed.

Let us now consider what effect chiral symmetry breaking may have on the differential cross sections. For simplicity, we will follow the studies of Refs. 3,4,5,6 to assume that chiral symmetry breaking will only modify the E_{0+} amplitude (although there is no reason to believe why higher multipoles can not be modified). As discussed above, the main effect of E_{0+} is through its interference with the dominant p-wave multipoles (see Table 1). For a more realistic estimate, we therefore include the 20% suppression of p-wave multipoles in this analysis. This assures that the fits (dashed curves in Fig. 2) to the magnitudes of the data are reasonable and hence the non-E_{0+} background amplitude is realistic. The effect on the calculated cross sections of adding $\pm 0.5 \times 10^{-3} m_\pi^{-1}$ to the E_{0+} amplitude, is illustrated in the dashed and dash-dotted curves of Fig. 4. We see that the change in E_{0+} significantly alters the angular distributions at the forward and backward angles. The magnitudes in the region near 90° are virtually unchanged. It is clear that more accurate experiments are needed for a quantitative determination of chiral symmetry breaking effects on the E_{0+} amplitude.

In conclusion, we have carried out a chiral invariant calculation of π^0 photo-production on the nucleon. It was achieved by inserting the meson-exchange πN model of Pearce and Jennings[14] into the gauge invariant and unitary Hamiltonian formulation of Nozawa,

Blankleider and Lee.[11] The calculated final state interaction effects strongly suppress the E_{0+} from the value predicted by the low energy theorem. Our results suggest that the effects of the imaginary part of E_{0+} and of the $l \geq 2$ multipoles should be included in multipole analyses of the data. As illustrated in Fig. 4, the experimental data is not yet accurate enough to enable a measurement of the degree of chiral symmetry breaking.

We would like to thank W. Weise for useful discussions. This work was supported in part by the U.S. Department of Energy, Nuclear Physics Division, under contract W-31-109-ENG-38, and by the Natural Sciences and Engineering Research Council of Canada.

References

[1]R. Beck *et al.* , Phys. Rev. Lett. **65**, 1841 (1990).

[2]E. Mazzucato *et al.* , Phys. Rev. Lett. **57**, 3144 (1986).

[3]D. Drechsel and L. Tiator, Phys. Lett. **B148**, 413 (1984).

[4]L.M. Nath and S.K. Singh, Phys. Rev. C **39**, 1207 (1989).

[5]Z.-J. Cao and L.S. Kisslinger, Phys. Rev. Lett. **64**, 1007 (1990).

[6]T. Schäfer and W. Weise, University of Regensburg preprint TPR-90-49.

[7]M. Araki, Phys. Lett. **B219**, 135 (1989).

[8]S. Nozawa, T.-S.H. Lee and B. Blankleider, Phys. Rev. C **41**, 213 (1990).

[9]S.N. Yang, Phys. Rev. C **40**, 1010 (1989).

[10]A.N. Kamal, Phys. Rev. Lett. **63**, 2364 (1989).

[11]S. Nozawa, B. Blankleider, and T.-S. H. Lee, Nucl. Phys. **A513** 459, (1990).

[12]B.W. Lee, Nucl. Phys. **B9**, 649 (1969); J.L. Gervais and B.W. Lee, *ibid.* **B12**, 627 (1969).

[13]W.-L. Lin and R.S. Wiley, Phys. Rev. D **14**, 196 (1976).

[14]B.C. Pearce and B.K. Jennings, submitted to Nucl. Phys. A.

[15]A.W. Thomas, Adv. in Nucl. Phys. **13**, 1 (1984).

[16]T.-S. H. Lee and B. Pearce, in preparation.

[17]D. Menze, W. Pfeil and R. Wilcke, ZAED Compilation of pion photoproduction Data, University of Bonn 1977.

Tables

TABLE I. The calculated complex s- p- and d-wave multipoles (in units of $10^{-3}m_{\pi}^{-1}$).

E_γ	E_{0+}	E_{1+}	M_{1+}	M_{1-}
146.8	(-0.6561, 0.0058)	(0.0859, 0.0000)	(1.3840, 0.0000)	(-0.3791, 0.0000)
149.1	(-0.4958, 0.0128)	(0.1275, 0.0002)	(2.0740, 0.0028)	(-0.5060, 0.0000)
151.4	(-0.0598, 0.0232)	(0.1349, 0.0003)	(2.5010, 0.0055)	(-0.6776, 0.0000)
153.7	(-0.0480, 0.5250)	(0.1492, 0.0000)	(2.9290, 0.0108)	(-0.7983, 0.0013)
156.1	(-0.0935, 0.7403)	(0.1632,-0.0007)	(3.3620, 0.0201)	(-0.8786, 0.0020)
E_γ	E_{2+}	E_{2-}	M_{2+}	M_{2-}
146.8	(-0.04516,-0.0000)	(-0.0004,-0.0000)	(0.0883, 0.0000)	(-0.1346,-0.0005)
149.1	(-0.06741,-0.0000)	(-0.0007,-0.0000)	(0.1306, 0.0000)	(-0.2002,-0.0009)
151.4	(-0.07401,-0.0000)	(-0.0007,-0.0000)	(0.1416, 0.0000)	(-0.2189,-0.0001)
153.7	(-0.08426,-0.0000)	(-0.0008,-0.0000)	(0.1599, 0.0000)	(-0.2485,-0.0018)
156.1	(-0.09563,-0.0000)	(-0.0010,-0.0000)	(0.1803, 0.0000)	(-0.2814,-0.0029)

Figures

FIG. 1. The calculated s-wave πN phases are compared with the data. Also shown are the isospin-odd and isospin-even s-wave scattering lengths (labeled S^- and S^+ respectively) plotted as functions of the pion mass.

FIG. 2. Results for the differential cross sections. The dashed curves are obtained by weakening the calculated p-wave multipoles by 20%. The data are from Ref. 17 ($E_\gamma \geq 159$ MeV) and Ref. 1 ($E_\gamma \leq 156.1$ MeV).

FIG. 3. The calculated E_{0+} amplitude near threshold.

FIG. 4. The effect on the differential cross sections of adding (dashed curves) and subtracting (dash-dotted curves) $0.5 \times 10^{-3} m_\pi^{-1}$ to the E_{0+} amplitude.

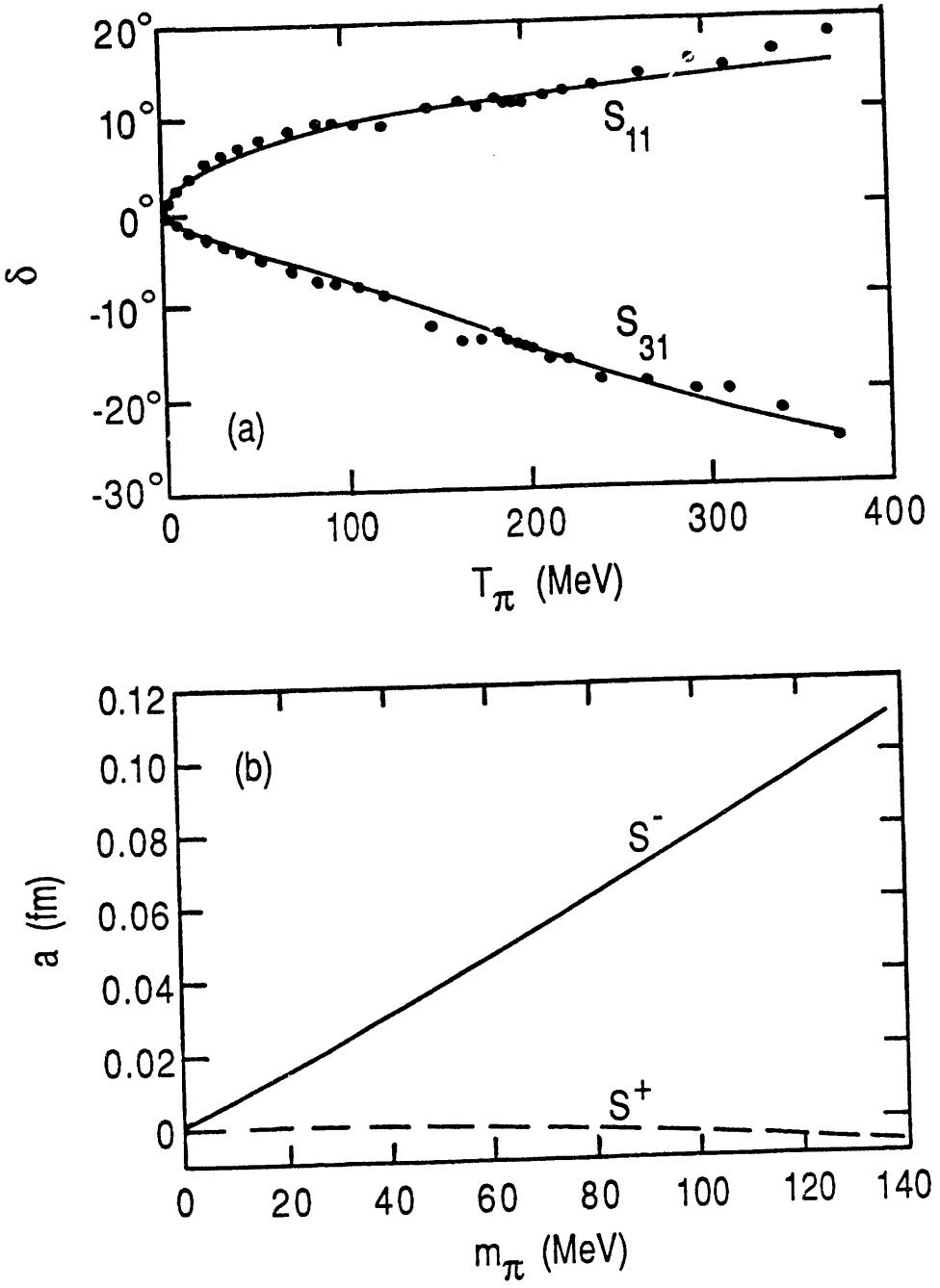
20°
10°
0°
-10°
-20°
-30°
δ
S11
S31
(a)
0
100
200
300
400
Tπ (MeV)
0.12
0.10
0.08
0.06
0.04
0.02
0
a (fm)
(b)
S-
S+
0
20
40
60
80
100
120
140
mπ (MeV)

Fig. 1

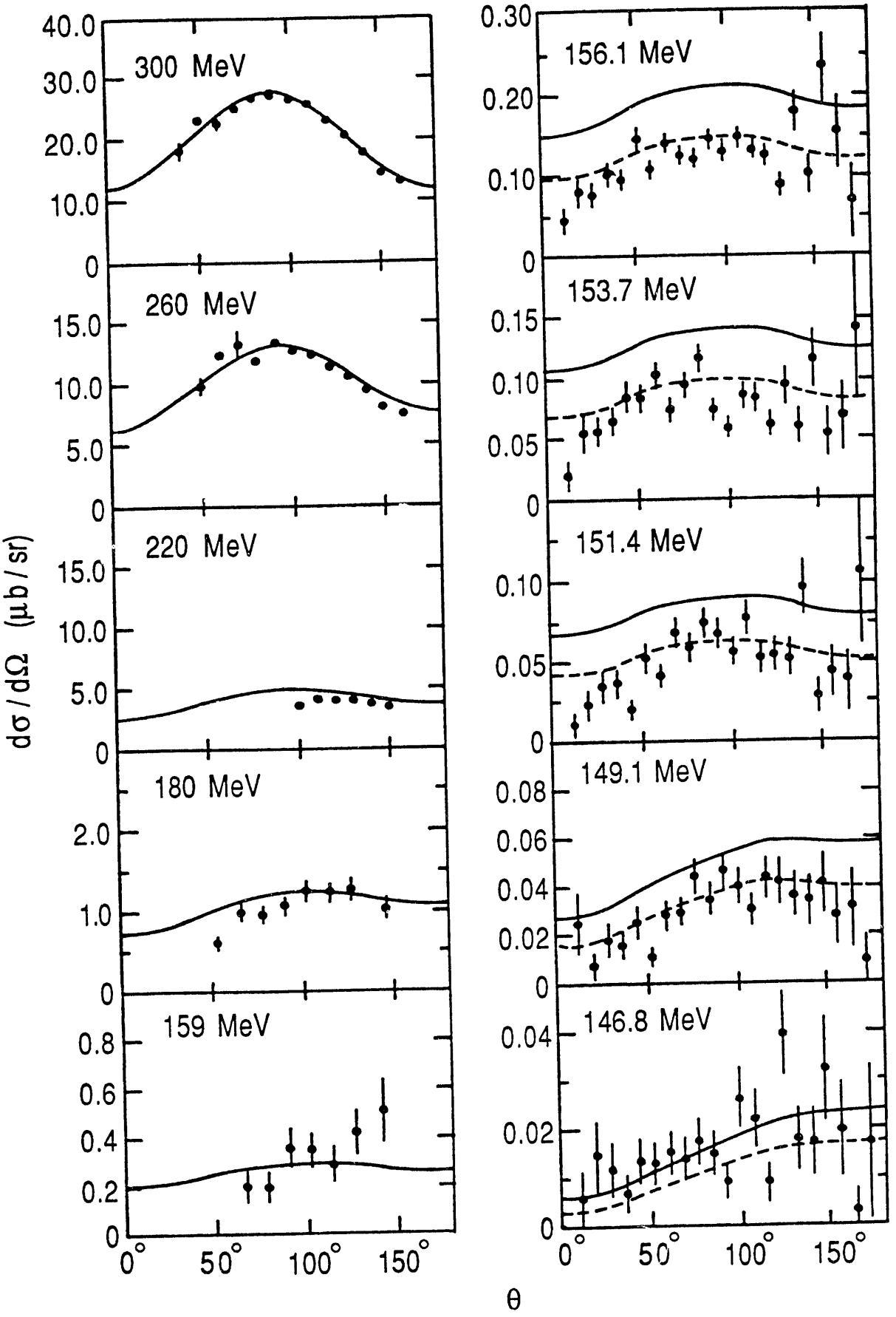
300 MeV
260 MeV
220 MeV
180 MeV
159 MeV
156.1 MeV
153.7 MeV
151.4 MeV
149.1 MeV
146.8 MeV
dσ/dΩ (μb/sr)
θ
0°
50°
100°
150°

Fig. 2

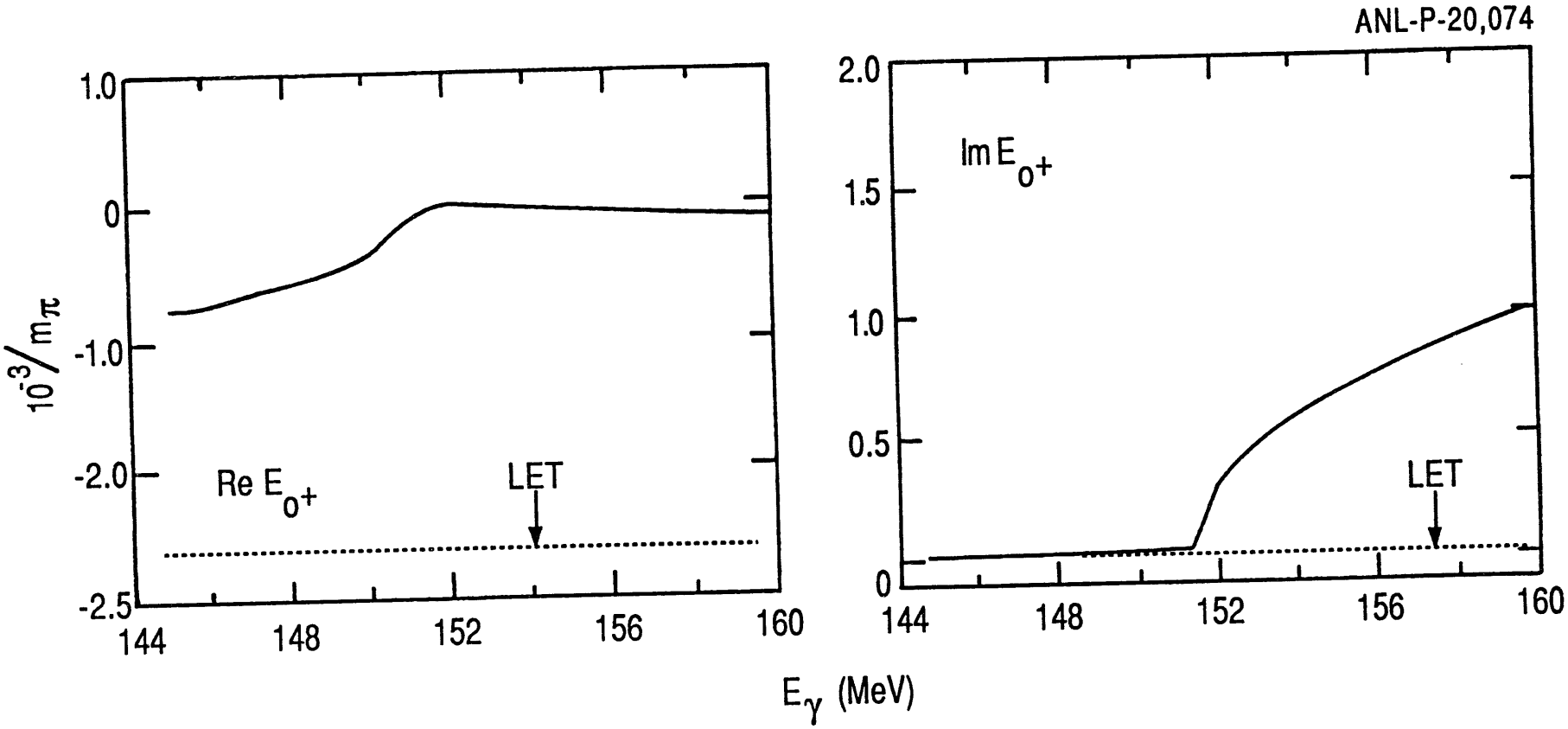
ANL-P-20,074
1.0
0
-1.0
-2.0
-2.5
$10^{-3}/m_\pi$
Re E_{0+}
LET
144
148
152
156
160
2.0
1.5
1.0
0.5
0
Im E_{0+}
LET
144
148
152
156
160
E_γ (MeV)

Fig. 3

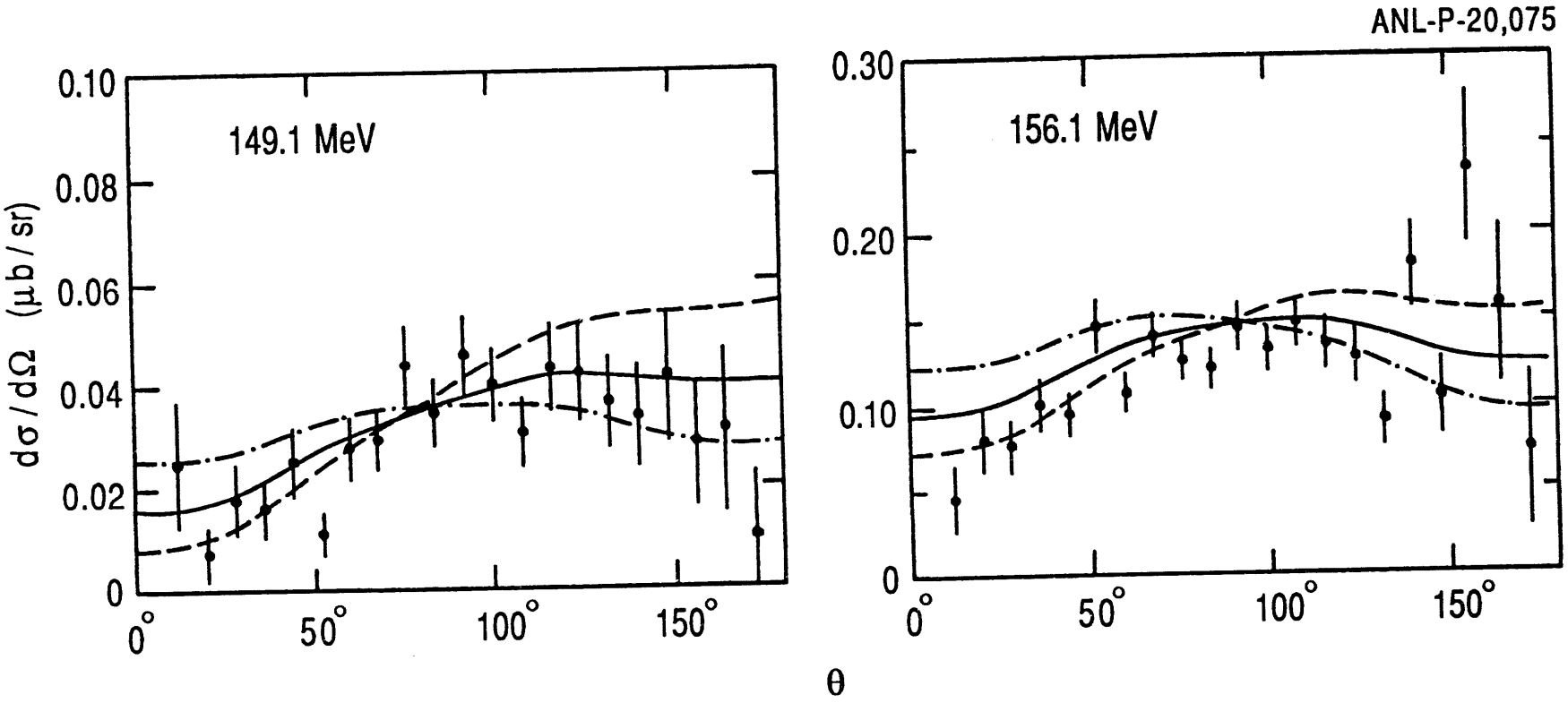
ANL-P-20,075
149.1 MeV
156.1 MeV
dσ/dΩ (μb/sr)
θ
0.10
0.08
0.06
0.04
0.02
0
0.30
0.20
0.10
0°
50°
100°
150°

Fig. 4

DATE FILMED

4/8/94

END